PHYSICAL REVIEW B **96**, 180403(R) (2017)

Microscopic reversal magnetization mechanisms in CoCrPt thin films with perpendicular magnetic anisotropy: Fractal structure versus labyrinth stripe domains

D. Navas,[1,*] N. Soriano,[2] F. Béron,[3] C. T. Sousa,[1] K. R. Pirota,[3] J. Torrejon,[3] C. Redondo,[2] R. Morales,[4,5] and C. A. Ross[6]

[1]*IFIMUP-IN and Departamento de Física e Astronomia, Universidade do Porto, 4169-007 Porto, Portugal*

[2]*Department of Chemical-Physics, University of the Basque Country UPV/EHU, 48940 Leioa, Spain*

[3]*Universidade Estadual de Campinas, Instituto de Fisica Gleb Wataghin, BR-13083970 Campinas, SP, Brazil*

[4]*Department of Chemical-Physics and BCMaterials, University of the Basque Country UPV/EHU, 48940 Leioa, Spain*

[5]*IKERBASQUE, Basque Foundation for Science, 48011 Bilbao, Spain*

[6]*Department of Materials Science and Engineering, Massachusetts Institute of Technology, Cambridge, Massachussets 02139, USA*

(Received 27 June 2017; revised manuscript received 18 September 2017; published 7 November 2017)

The magnetization reversal of CoCrPt thin films has been examined as a function of thickness using magneto-optical Kerr effect (MOKE) microscopy and first-order reversal curves (FORC) techniques. MOKE images show differentiated magnetization reversal regimes for different film thicknesses: while the magnetic domains in 10-nm-thick CoCrPt film resemble a fractal structure, a labyrinth stripe domain configuration is observed for 20-nm-thick films. Although FORC distributions for both cases show two main features related to irreversible processes (propagation and annihilation fields) separated by a mostly flat region, this method can nonetheless distinguish which magnetization reversal process is active according to the horizontal profile of the first FORC peak, or propagation field. A single-peak FORC profile corresponds to the fractal magnetization reversal, whereas a flat-peak FORC profile corresponds to the labyrinth magnetization reversal.

DOI: 10.1103/PhysRevB.96.180403

I. INTRODUCTION

Since the middle of the 1970s, when Iwasaki *et al.* proposed perpendicular magnetic recording as an alternative to conventional longitudinal magnetic recording [1–3], thin films with out-of-plane magnetic anisotropy have been widely studied for recording media applications [4–7] as well as for patterned magnetic media [8–11]. Magnetic films with perpendicular magnetic anisotropy (PMA) patterned into stripes and lines [12–15] have been also proposed for nanoscale spintronic devices such as those based on current-driven domain-wall motion [16,17]. Moreover, magnetic skyrmions, the smallest known spin textures in magnetic thin films, have been recently stabilized at room temperature [18] in systems with PMA and have also been electrically manipulated [19], which opens the path toward skyrmionic devices [20].

Co-based alloys and multilayers have been widely used for the recording layer in perpendicular media. CoCr alloy thin films were proposed in 1979 [2], and many Co alloys, including CoCrPt, CoCrTa, CoCrNb, CoCrPtNb, and CoCrPtB, have been studied [21]. However, in order to successfully implement them into technological applications, a detailed understanding of their magnetization reversal process is required. The out-of-plane reversal processes of ferromagnetic thin films with PMA is usually described by the nucleation of reverse domains when the magnetic field reaches the nucleation field (H_n), followed by an avalanchelike growth until residual unreversed or bubble domains are finally annihilated at the annihilation field (H_A) [22]. However, several works have already shown that the magnetization reversal is a rather complex phenomenon. Davies *et al.* [23] observed that the magnetization reversal of Co/Pt multilayers is dominated by irreversible processes corresponding to the avalanchelike propagation of one-dimensional stripe domains originated from earlier nucleated zero-dimensional bubble domains. This was obtained using the first-order reversal curves (FORC) technique in combination with transmission x-ray microscopy and resonant x-ray small-angle scattering. Im *et al.* [24,25] studied the nucleation process via individual Barkhausen avalanches in 50-nm-thick $(Co_{0.83}Cr_{17})_{87}Pt_{13}$ alloy films through magnetic soft x-ray transmission microscopy. Schwarz *et al.* [26] examined the mechanisms of the reversal processes by the detection of individual Barkhausen jumps on the nanometer scale in granular $La_{0.7}Sr_{0.3}MnO_3$ thin films using ultrahigh-vacuum low-temperature magnetic force microscopy (MFM).

Here, we have examined the complex reversal magnetization of $Co_{66}Cr_{22}Pt_{12}$ (CoCrPt) thin films with PMA. This Co-based alloy has uniaxial magnetocrystalline anisotropy and the crystalline *c* axis can be oriented out of plane by epitaxial growth onto a Ti (0001) underlayer [27–29]. In prior works, we showed that the hysteresis loops of both 10- and 20-nm-thick CoCrPt thin films had out-of-plane remanence ratio ≈ 1, and an in-plane hard axis [28,29]. MFM of ac-demagnetized 20-nm-thick CoCrPt films showed a maze domain structure, typical of thin films with out-of-plane anisotropy, and with an average domain size of (180 ± 10) nm [28,30] (the 10-nm film could not be imaged since the stray field of the MFM tip significantly modified the domain patterns). Moreover, using MFM, polarized neutron reflectometry, and micromagnetic simulations, we determined that while the domain walls in 20-nm-thick CoCrPt films consist of a Bloch wall in the center of the thin film with a pair of Néel caps at the surfaces, the 10-nm-thick film exhibits pure Bloch walls [28].

In this Rapid Communication we analyze magnetization reversal for these two film thicknesses using FORC and magneto-optical Kerr effect (MOKE) microscopy techniques. FORC measurements consist of several minor hysteresis loops, beginning at different reversal fields H_r and going back to positive saturation. The FORC distribution ρ represents

*Corresponding author: davidnavasotero@gmail.com

the statistical distribution of the system of hysterons. It can be calculated through a second-order mixed derivative of magnetization M with respect to applied fields H and H_r [31]:

$$\rho(H,H_r) = -\frac{1}{2}\frac{\partial^2 M}{\partial H\,\partial H_r}\ (H \geqslant H_r). \qquad (1)$$

As this derivative eliminates the purely reversible components of the magnetization ($\rho = 0$) [32], any nonzero ρ corresponds to irreversible processes [23]. Therefore, this technique is suitable for studying irreversible local events such as individual Barkhausen jumps.

As pointed out in [24,25], few experiments have been performed on Barkhausen avalanches in nucleation-mediated magnetization reversal processes of PMA materials, mainly due to the low sensitivity and limited spatial resolution of measurement techniques. This study shows that CoCrPt exhibits different magnetization reversal regimes as a function of thickness via MOKE and demonstrates that FORC can provide a convenient diagnostic for the reversal and for quantifying both the propagation and annihilation fields. Although we must be aware that the sample set is limited, we do believe it can be generally applied to samples with PMA and provides another approach to determine the magnetization reversal mechanisms of this kind of system using a standard magnetometry technique such as FORC analysis.

II. EXPERIMENTAL SECTION

A 5-nm Ti seed layer, 10- or 20-nm-thick $Co_{66}Cr_{22}Pt_{12}$ film, and a 3-nm Ti capping layer were deposited sequentially by rf sputtering at room temperature on Si substrate (more details are given in Ref. [30]). The film thicknesses were determined by performing atomic force microscopy measurements. Room-temperature magnetic hysteresis loops and FORC diagrams were measured in a vibrating sample magnetometer (VSM), and domain images were obtained from MOKE microscopy using a light-emitting diode lamp with white light spectrum. The precision of the FORC diagram is governed by the magnetic field and reversal field steps, ΔH and ΔH_r, respectively. In this work, we selected values for saturation field H_{sat} of 5 kOe, $\Delta H = 5$ and 25 Oe, and $\Delta H_r = 5$ and 10 Oe, based on the major hysteresis loops of 10- and 20-nm-thick film, respectively. In order to reduce the presence of dynamical or thermal activation effects [33,34], FORCs were measured using low field sweep rates such as 0.125 and 1.25 Oe/s, for 10- and 20-nm-thick CoCrPt films, respectively. For the same reason, we used a stabilization rate of 1 Oe/s for MOKE measurements in both samples.

III. RESULTS AND DISCUSSION

From the out-of-plane major hysteresis loops (Figs. 1 and 2), we determine that the 10-nm-thick film has nominal nucleation and coercive fields of (82 ± 5) and (98 ± 5) Oe, respectively, whereas the 20-nm-thick film shows values of (72 ± 5) and (140 ± 5) Oe. Although saturation occurs via domain annihilation in both samples, the hysteresis loop shape is almost square for the 10-nm-thick film (Fig. 1), while the 20-nm-thick film (Fig. 2) shows a slow approach to saturation that was attributed to the existence of residual bubble domains.

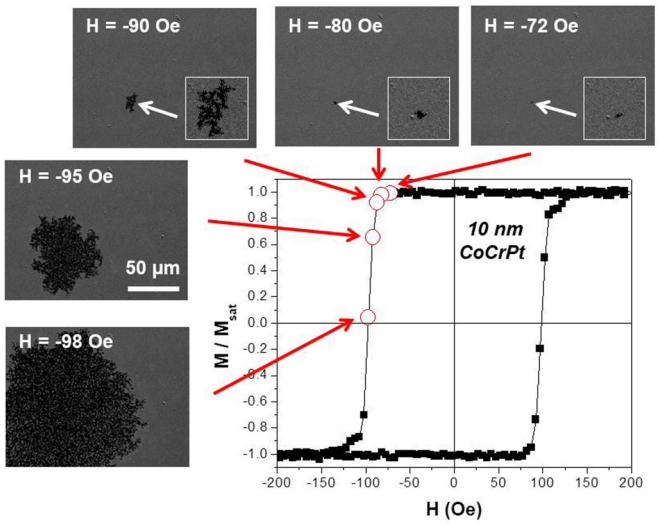

FIG. 1. Out-of-plane (■) hysteresis loops of 10-nm-thick CoCrPt film along with MOKE images. In images with applied fields of −72, −80, and −90 Oe, magnified images ($20 \times 20\ \mu m^2$) of the reversed domains are shown in the insets and pointed out by white arrows. Reversed domains ("down") are highlighted in black.

To assess the details of the reversal, MOKE microscopy was used to obtain the out-of-plane hysteresis loops and their related Kerr images over a $177 \times 136\ \mu m^2$ area (Figs. 1 and 2). The bright-dark contrast illustrates the opposite "up"-"down" domains. Although the spatial resolution limit of our MOKE microscope does not allow us to achieve a detailed study of the reversal process and the magnetic domains were only visible once they reach a size of a few hundred nanometers, the morphology development and density of these domains were clearly resolved once they reach this critical size. When the external applied field is +300 Oe, the 10-nm-thick sample (Fig. 1) is fully saturated according to both macroscopic (VSM) and microscopic (MOKE microscopy) measurements.

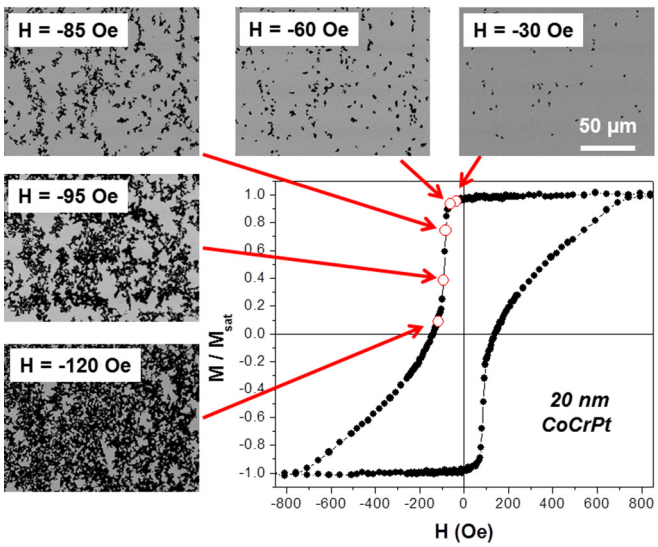

FIG. 2. Out-of-plane (●) hysteresis loops of 20-nm-thick CoCrPt film along with MOKE images. Reversed domains ("down") are highlighted in black.

Although the magnetization remains high until the reversal field reaches the nominal nucleation field (-82 ± 5) Oe, isolated nucleation of reverse domains was already observed at (-72 ± 2) Oe. As was previously commented, the identification of reverse domains is limited by the spatial resolution limit of the MOKE microscope, but the measurements show that the reversal process starts by the nucleation of well-separated spotlike bubble domains (with $\approx$1 nucleation site/0.02 mm^2) that grow in size with increasing field magnitude with a shape resembling a fractal structure, until the entire sample is almost reversed. Remaining isolated domains are annihilated and the sample is fully saturated at a larger reverse field $(-150 \pm 5$ Oe).

For the 20-nm-thick sample (Fig. 2), the VSM indicates a nominal nucleation field of (-72 ± 5) Oe, but reverse domains can be seen at (-30 ± 2) Oe via MOKE. The reversal process starts by the nucleation of bubble domains (a few tens of nucleation sites/0.02 mm^2 area). Increasing nucleation is seen in the field range from -30 to -60 Oe, and as the field magnitude continues to increase the domains expand into stripes [23] that form a labyrinth pattern covering the film. The slow approach to saturation corresponds to the growth of the stripe domains until unreversed isolated domains are annihilated, $(-750 \pm 25$ Oe). Thus the 20-nm-thick film has a much higher nucleation density of reverse domains than the 10-nm-thick film.

While major hysteresis loops give averaged properties such as coercivity and reduced remanence, the FORC technique uses a larger data set providing much more detailed information about the reversal process of a system such as those fields at which irreversible events occur. FORC distributions are shown in Figs. 3(a) and 3(b) for 10- and 20-nm-thick films, respectively. Both cases show three main features labeled as

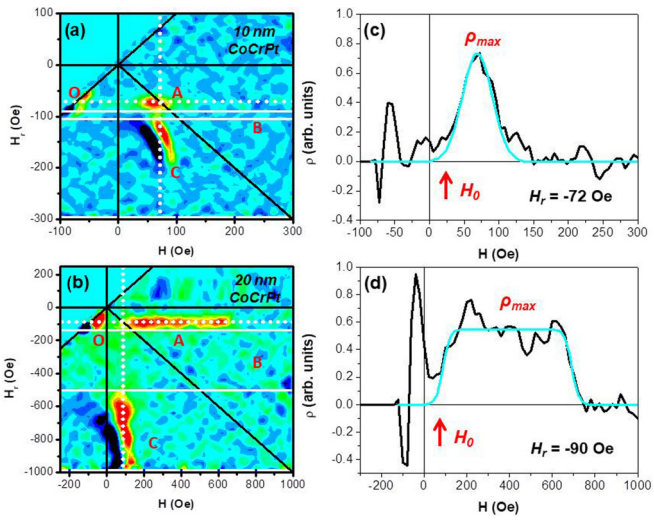

FIG. 3. FORC distributions of (a) 10-nm-thick and (b) 20-nm-thick CoCrPt films. The color scale of the FORC diagrams ranges from light blue to red for $\rho > 0$ and from light blue to black for $\rho < 0$. (c),(d) Profiles along the horizontal dashed lines in Figs. 3(a) and 3(b) of peak A of the FORC diagrams for (c) 10-nm-thick and (d) 20-nm-thick CoCrPt films. In light blue, and as a guide to the eye, we plotted simplified diagrams of the FORC profiles for both 10-nm-thick (c) and 20-nm-thick (d) films.

A, B, and C. While peak A is a positive ρ distribution that is elongated along the external applied field direction (horizontal distribution), peak C is formed by a positive/negative ρ distribution elongated along the reversal field axis (vertical distribution). Both features are related to irreversible processes and they are separated by a region with $\rho \sim 0$ marked as B, between white horizontal lines in Figs. 3(a) and 3(b).

As described in prior works [23,35–38], thin films with perpendicular anisotropy show similar FORC distributions. Peak A is an irreversible process corresponding to the nucleation and propagation of reverse domains. This process occurs at $H_{\text{prop}} \approx (-72 \pm 20)$ Oe and $\approx (-90 \pm 10)$ Oe for 10- and 20-nm-thick films, respectively. Then, FORC diagrams show a reversible region (region B, between the white horizontal lines in Figs. 3(a) and 3(b)) that is associated with the expansion and contraction of domains. It corresponds to the slow approach to saturation observed in the hysteresis loops and it is significantly wider for 20-nm-thick film ($-500 < H_r < -140$ Oe) than for the 10-nm-thick film ($-105 < H_r < -90$ Oe). Finally, the vertical positive/negative ρ distribution (peak C) is related to the annihilation of remaining domains (H_A), and a nonzero ρ is present until all of the remaining domains are completely eliminated. In this regime, the FORC curves return by nucleation/growth/rotation processes in which each curve shows a new propagation field (H_{prop^*}), lower than H_{prop}, since the magnetization change is favored at preexisting unreversed domains [23,38]. This assertion is supported by the slight inclination of distribution C versus the vertical axis. At the bottom of distribution C (i.e., when coming back from a negative fully saturated system), H_{prop^*} (dashed vertical white lines in Figs. 3(a) and 3(b)) is finally equal to H_{prop} (dashed horizontal white lines in Figs. 3(a) and 3(b)). Irreversible processes persist well beyond the apparent saturation field (H_{sat}), at which saturation is nominally reached in the hysteresis loops [23,38], and larger fields, such as $H_r \approx -200$ Oe and ≈ -1000 Oe for 10- and 20-nm-thick CoCrPt film, respectively, are required to fully saturate the CoCrPt.

Finally, our analysis focuses on the shape of peak A (Figs. 3(c) and 3(d)). When H_r reaches H_{prop}, and reversed domains are already nucleated, the magnetization behavior until the sample is resaturated shows a clear fingerprint for distinguishing between the kind of domain configuration that was generated. To illustrate this, we examine the FORC minor loops and MOKE images (Figs. 4 and 5) as well as the horizontal profiles along peak A (Figs. 3(c) and 3(d)).

In the 10-nm-thick film minor loop (red branch in Fig. 4), when H_r is larger than H_{prop}, the magnetization continues to fall even after the magnetic field begins to increase between -75 and -65 Oe. This drop is assumed to occur because once reverse domains are nucleated, they grow by following an avalanchelike process [39], which is confirmed by MOKE images in Figs. 4(a) and 4(b). Afterward, a large plateau with almost constant magnetization occurs from -65 to 34 Oe, followed by a second step with large susceptibility. This behavior is compared with a pinning type magnet consisting of isolated magnetic moments with a specific coercive field [22]. The FORC profile along peak A ($H_r = (-72 \pm 20)$ Oe) shows four stages (Fig. 3(c)):

(1) Initially, a negative/positive ρ distribution occurs (feature O of the FORC distribution in Fig. 3(a)) associated with

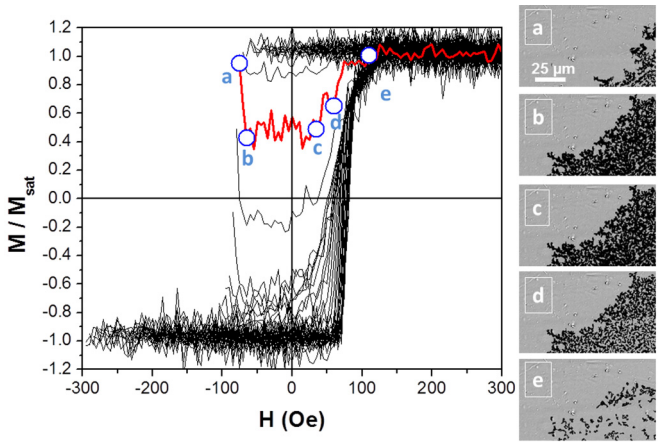

FIG. 4. Minor hysteresis loops of 10-nm-thick CoCrPt film along with MOKE images at different steps along the minor loop indicated in red ($a = -75$ Oe; $b = -65$ Oe; $c = +34$ Oe; $d = +60$ Oe; $e = +110$ Oe).

the magnetization drop at the beginning of the minor hysteresis loops. This is a dynamical effect related to the fact that once the avalanchelike reversal process starts, reversed domains grow even if the magnetic field is increased. Although we measured the first-order reversal curves using low field sweep rates, dynamical effects are still observed. However, as Cornejo *et al.* [34] experimentally confirmed, the use of different field sweep rates exclusively modifies the FORC features related to dynamical effects without affecting the rest of the FORC distributions (such as *A*, *B*, and *C* in our samples).

(2) The ρ distribution tends to ≈ 0 and the sample magnetization is constant until a critical field is reached (H_0). During this step, the domain configuration is stable because the magnetostatic energy is balanced against the exchange and magnetocrystalline anisotropy terms (Fig. 4(c)).

(3) The ρ distribution increases to $\rho_{\max}$, which is associated with the growth in size of the unreversed domains inside the fractal structure leaving small reverse domains (Fig. 4(d)).

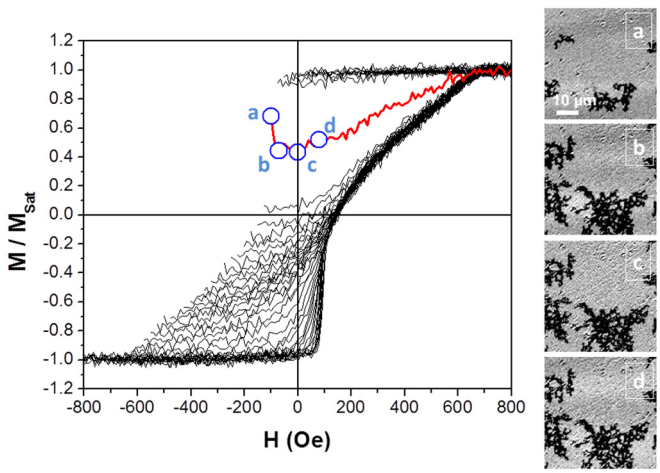

FIG. 5. Minor hysteresis loops of 20-nm-thick CoCrPt film along with MOKE images at different steps along the minor loop indicated in red ($a = -100$ Oe; $b = -70$ Oe; $c = 0$ Oe; $d = +80$ Oe).

(4) Finally, ρ decreases, as a consequence of the size reduction of the reversed spots until the sample is fully resaturated (Fig. 4(e)).

The 20-nm-thick film minor loop (red branch in Fig. 5) also shows an initial magnetization drop (between -100 and -70 Oe) followed by a plateau with low susceptibility between -70 and 0 Oe. From 0 Oe to resaturation, the susceptibility is almost constant and is associated with domain-wall motion [22]. The FORC profile along peak $A(H_r = (-90 \pm 10)$ Oe) presents three main stages (Fig. 3(d)):

(1) Again, the magnetization drop, originated by dynamical effects, leads to a negative/positive ρ distribution (feature *O* of the FORC distribution in Fig. 3(b); see also Figs. 5(a) and 5(b)).

(2) The ρ distribution is ≈ 0 and no reversal process is observed, implying that the labyrinth configuration is stable (Fig. 5(c)).

(3) Finally, after a critical field is reached (H_0), the ρ distribution increases up to a constant positive value ($\rho_{\max}$), indicating that the size of the reversed stripe domains is reduced by magnetization rotation until the sample is resaturated at ~ 700 Oe (Fig. 5(d)).

Therefore, we suggest that while a single-peak FORC profile corresponds to the magnetization reversal process proceeding via a fractal structure originating from sparse nucleation sites, a flat-peak FORC profile represents the magnetization reversal process via a labyrinth stripe domain configuration with denser nucleation sites for reversal [23].

Although an imaging technique with high sensitivity and spatial resolution is always the best option to achieve a detailed study of the reversal process of systems with PMA, these techniques, such as x-ray microscopy, resonant x-ray small-angle scattering, or ultrahigh-vacuum low-temperature magnetic force microscopy, are not widely available. This actually motivates the use of more standard techniques such as FORC measurements, to distinguish between the different reversal processes.

In summary, we have studied the magnetization reversal of 10- and 20-nm-thick CoCrPt films. The major hysteresis loops confirm the out-of-plane easy magnetization direction but give little insight into the details of the reversal process. MOKE images show that the reversal of a 10-nm-thick CoCrPt film follows a fractal structure developing from sparse nucleation reversal sites, instead of the labyrinth stripe domain configuration developing from denser nucleation reversal sites observed for a 20-nm-thick film, and FORC measurements show qualitative differences between the two thicknesses. The shape of the horizontal profiles of the FORC distribution (Figs. 3(c) and 3(d)) along the first irreversible feature, peak *A* (horizontal dashed lines in Figs. 3(a) and 3(b)), shows that a single-peak FORC profile corresponds to magnetization reversal via fractal domains, whereas a flat-peak FORC profile corresponds to magnetization reversal via labyrinth stripe domains.

In this work the only variable was the film thickness, but varying thickness does naturally lead to changes in other parameters such as grain size, defects, effective anisotropy, etc. Although our microstructural studies, using x-ray analysis and polarized neutron reflectometry [28,29], did not show differences with the CoCrPt thicknesses and deeper analysis could be required, we have determined that while the domain

walls in 20-nm-thick CoCrPt films consist of a Bloch wall in the center of the thin film with a pair of Néel caps at the surfaces, the 10-nm-thick film exhibits pure Bloch walls [28]. This behavior is related to the competition between exchange interactions, keeping spins parallel, magnetic anisotropy orienting magnetization normal to the surface, and demagnetizing fields, promoting in-plane magnetization. Assuming that both exchange interactions and magnetocrystalline anisotropy are independent of the film thickness, the increase of demagnetizing fields [40] could justify the presence of different domain-wall configurations as a function of film thickness. According to this, we suggest that while pure Bloch walls favor the magnetization reversal via fractal domains in 10-nm-thick films, Bloch walls, with Néel caps at the surfaces, promote magnetization reversal via labyrinth stripe domains.

Therefore, we have related a macroscopic measurement (FORC) to the microscopically measured domain evolution (MOKE imaging) and explained why the different nucleation/growth processes evident in MOKE lead to different features in the FORC distributions. In conclusion, we have demonstrated that FORC distributions provide clear fingerprints for the reversal processes of PMA films and we believe that this methodology can be generally applied to samples with PMA.

ACKNOWLEDGMENTS

This work was supported by Spanish Grants No. AEI FIS2013-45469 and No. AEI FIS2016-76058, and UE FEDER "Una manera de hacer Europa", the European Union's Horizon 2020 research and innovation programme under the Marie Sklodowska-Curie Grant Agreement No. 734801. D.N. thanks Fundaçao para a Ciência e Tecnologia (Contract No. IF/01191/2013) for financial support.

[1] S. Iwasaki and Y. Nakamura, IEEE Trans. Magn. **14**, 436 (1978).
[2] S. Iwasaki, Y. Nakamura, and K. Ouchi, IEEE Trans. Magn. **15**, 1456 (1979).
[3] S. Iwasaki, IEEE Trans. Magn. **20**, 657 (1984).
[4] H. J. Richter, J. Phys. D **40**, R149 (2007).
[5] J. H. Judy, J. Magn. Magn. Mater. **287**, 16 (2005).
[6] S. N. Piramanayagam and K. Srinivasan, J. Magn. Magn. Mater. **321**, 485 (2009).
[7] R. Wood, J. Magn. Magn. Mater. **321**, 555 (2009).
[8] B. D. Terris and T. Thomson, J. Phys. D **38**, R199 (2005).
[9] M. Albrecht, A. Moser, C. T. Rettner, S. Anders, T. Thomson, and B. D. Terris, Appl. Phys. Lett. **80**, 3409 (2002).
[10] A. Moser, O. Hellwig, D. Kercher, and E. Dobisz, Appl. Phys. Lett. **91**, 162502 (2007).
[11] K. Naito, Chaos **15**, 047507 (2005).
[12] D. Ravelosona, D. Lacour, J. A. Katine, B. D. Terris, and C. Chappert, Phys. Rev. Lett. **95**, 117203 (2005).
[13] C. Burrowes, A. P. Mihai, D. Ravelosona, J.-V. Kim, C. Chappert, L. Vila, A. Marty, Y. Samson, F. Garcia-Sanchez, L. D. Buda-Prejbeanu, I. Tudosa, E. E. Fullerton, and J.-P. Attané, Nat. Phys. **6**, 17 (2010).
[14] E. Martinez, Adv. Condens. Matter Phys. **2012**, 954196 (2012).
[15] S. Emori, U. Bauer, S.-M. Ahn, E. Martinez, and G. S. D. Beach, Nat. Mater. **12**, 611 (2013).
[16] S. S. P. Parkin, M. Hayashi, and L. Thomas, Science **320**, 190 (2008).
[17] D. A. Allwood, G. Xiong, C. C. Faulkner, D. Atkinson, D. Petit, and R. P. Cowburn, Science **309**, 1688 (2005).
[18] C. Moreau-Luchaire, C. Moutafis, N. Reyren, J. Sampaio, C. A. F. Vaz, N. Van Horne, K. Bouzehouane, K. Garcia, C. Deranlot, P. Warnicke, P. Wohlhüter, J.-M. George, M. Weigand, J. Raabe, V. Cros, and A. Fert, Nat. Nanotechnol. **11**, 444 (2016).
[19] S. Woo, K. Litzius, B. Krüger, M-Y. Im, L. Caretta, K. Richter, M. Mann, A. Krone, R.M. Reeve, M. Weigand, P. Agrawal, I. Lemesh, M-A. Mawass, P. Fischer, M. Kläui, and G. S. D. Beach, Nat. Mater. **15**, 501 (2016).
[20] A. Fert, V. Cros, and J. Sampaio, Nat. Nanotechnol. **8**, 152 (2013).
[21] S. N. Piramanayagam, J. Appl. Phys. **102**, 011301 (2007).
[22] E. A. Jagla, Phys. Rev. B **72**, 094406 (2005).
[23] J. E. Davies, O. Hellwig, E. E. Fullerton, G. Denbeaux, J. B. Kortright, and K. Liu, Phys. Rev. B **70**, 224434 (2004).
[24] M.-Y. Im, P. Fischer, D.-H. Kim, K.-D. Lee, S. H. Lee, and S.-C. Shin, Adv. Mater. **20**, 1750 (2008).
[25] M.-Y. Im, P. Fischer, D.-Y. Kim, and S.-C. Shin, Appl. Phys. Lett. **95**, 182504 (2009).
[26] A. Schwarz, M. Liebmann, U. Kaiser, R. Wiesendanger, T. W. Noh, and D. W. Kim, Phys. Rev. Lett. **92**, 077206 (2004).
[27] N. Inaba, Y. Uesaka, and M. Futamoto, IEEE Trans. Magn. **36**, 54 (2000).
[28] D. Navas, C. Redondo, G. A. Badini Confalonieri, F. Batallan, A. Devishvili, Ó. Iglesias-Freire, A. Asenjo, C. A. Ross, and B. P. Toperverg, Phys. Rev. B **90**, 054425 (2014).
[29] D. Navas, L. Bi, A. O. Adeyeye, and C. A. Ross, Adv. Mater. Interfaces **2**, 1400551 (2015).
[30] D. Navas, C. Nam, D. Velazquez, and C. A. Ross, Phys. Rev. B **81**, 224439 (2010).
[31] C. R. Pike, A. P. Roberts, and K. L. Verosub, J. Appl. Phys. **85**, 6660 (1999).
[32] I. D. Mayergoyz, *Mathematical Models of Hysteresis* (Springer, New York, 1991).
[33] D. R. Cornejo, T. R. F. Peixoto, S. Reboh, P. F. P. Fichtner, V. C. de Franco, V. Villas-Boas, and F. P. Missell, J. Mater. Sci. **45**, 5077 (2010).
[34] D. R. Cornejo, R. D. Noce, T. R. F. Peixoto, N. Barelli, P. T. A. Sumodjo, and A. V. Benedetti, J. Alloys Compd. **479**, 43 (2009).
[35] A. Stancu, C. Pike, L. Stoleriu, P. Postolache, and D. Cimpoesu, J. Appl. Phys. **93**, 6620 (2003).
[36] J. Yin, H. Zhang, F. Hu, B. Shen, and L. Q. Pan, J. Appl. Phys. **106**, 103901 (2009).
[37] Z. Diao, N. Decorde, P. Stamenov, K. Rode, G. Feng, and J. M. D. Coey, J. Appl. Phys. **111**, 07B538 (2012).
[38] J. E. Davies, O. Hellwig, E. E. Fullerton, M. Winklhofer, R. D. Shull, and K. Liu, Appl. Phys. Lett. **95**, 022505 (2009).
[39] D. L. Mobley, C. R. Pike, J. E. Davies, D. L. Cox, and R. R. P. Singh, J. Phys.: Condens. Matter **16**, 5897 (2004).
[40] D. A. Gilbert, J.-W. Liao, B. J. Kirby, M. Winklhofer, C.-H. Lai, and K. Liu, Sci. Rep. **6**, 32842 (2016).